AIAA Atmospheric Flight Mechanics
Conference and Exhibit
6-9 August 2001 Montreal, Canada

A01-37231

AIAA-2001-4010

STATIC AND DYNAMIC ANALYSIS OF AN UNCONVENTIONAL PLANE: FLYING WING[1]

Sergio Esteban*
Department of Mechanical and Aerospace Engineering and Engineering Mechanics
University of Missouri-Rolla, Missouri 65401

Abstract

The need to investigate the static and dynamic stability for unconventional planes requires development of a code that automates the analysis for the airplane's stability performance. Flying wings are unconventional and challenging to analyze because they lack a tail to control the plane in the longitudinal and the lateral directions. With this motivation, an automated code was designed that was able to accurately predict the stability performance of flying wings. In general most of the stability derivatives that govern the dynamic behavior of an airplane are simplified so they would only include the terms that represent the greatest contribution to its final value. When the greatest contribution to any of the derivatives comes from the tail, and the airplane being analyzed lacks a tail, this represents a problem. This study tries to solve this problem by focusing on decoupling the longitudinal and lateral stability derivatives into its wing and vertical fin contributions.

Introduction

Through the centuries, men have always tried to conquer all possible areas of our planet: "By sea, land or air men will be there..." This last one has been one of the most challenging since Mother Nature and evolution decided that we should not have wings. For centuries we have admired, from a distance, the wonderful soaring of some of the most beautiful creatures: eagles, storks or condors to name a few. Our drive to conquer forbidden areas leaded our curiosity to the extreme trying to emulate those wonderful soaring kings of the skies. Probably one of the most significant hits in aviation history was that of the Wright brothers' flight on December 17th, 1903, when they accomplished the first heavier-than-air flight in history, but indeed this was not the first attempt. As early as the ancient Greeks, with the myth of Daedalus and his son Icarus men all over the world and time, have tried to emulate birds. In Italy, Michelangelo and his extravagant ornithopter flying devices in the late 15th century; in France, Montgolfier and his balloons in the late 18th; in England, Sir George Cayley with the first concept of a fixed-wing aircraft in the late 18th century and early 19th century; Otto Lilienthal and his gliders in the Germany of the late 19th century or Langley in the United States at the same time that the Wright brothers wrote history. These are among some of the men that have tried to rewrite history by literally dedicating their life to the pursuit of flying like birds.[1]

In the recent years a wide variety of unconventional planes have been soaring our skies, all of them trying to emulate the magnificent flight of the soaring kings of the skies. Not even the most agile and powerful of today fighters can be compared to the superb and delicate soaring of an eagle. The phrase, "A WING ALONE SUFFICES" has been long ago coined and used when designing airplanes with just a single wing with no tail. Whatever its name -"tailless aircraft", "flying wing aircraft", "flying wing" or "all-wing-aircraft"- they all represent the purest and closest design to the nature. It is important to define what airplanes fall under this definition. Nickel and Wohlfahrt limit the use of the term flying wing "...to be used only in the special case where there is no fuselage and no vertical fin(s)." Exceptions are made for planes with small vertical fins such those of the Northrop YB 49.[2] Some examples of historical flying wings are most of the Horten brothers' creations during the 1930's and throughout the century, the Lippisch's Storch models created in the years prior to the WWII, the lifting bodies created and tested by NASA from 1963 to 1975, or the Northrop B-35, the YB 49, predecessor of the latest and one of the most famous flying wing: the B-2 Spirit.

Tailless aircraft represent a distinct challenge when trying to predict their static and dynamic stability

* Graduate Student

performance since most of the literature that has been written on this subject is geared towards conventional planes. Conventional airplanes are those that consist of a wing and a tail structure for their control.

With this in mind, and as a part of a design proposal, a group of six student engineers, decided construct and fly an unconventional unmanned aircraft for aerial photography missions. The request for proposal (RFP) requested that the aircraft should be capable of taking photographs of objects on the ground from altitudes at least 500 feet with a radius of operation of at least of ¼ mile. The airplane was to be economical to construct and operate, and should not require exceptional piloting skills.[3] The decision was made to focus their efforts to accomplish the *RFP* requirements by means of a highly unconventional plane and a flying wing presented a distinct challenge when compared to traditional plane layouts. The group called themselves the *Tailless Wonders*, and called their plane *Ala Voladora*, which is Spanish for "flying wing". [4] Throughout this paper the plane will be referred as *Ala*.

The analysis stage of the *Tailless Wonders* design was divided in four major areas: aerodynamics, propulsion and performance, structures, and stability and control. This paper only focuses on the efforts that were made by the author and member of the *Tailless Wonders* to automate the analysis process conducted during the last eight months towards predicting the stability and control performance of *Ala* to obtain a plane that not only would be pilot-friendly, but also would be highly maneuverable. The other three major areas involved in the final product of *Ala*, aerodynamics, propulsion and performance, and structures, are not included in this paper but were of major importance during the entire analysis process since they also defined the layout for the plane.

After an initial aerodynamic and preliminary static stability analysis the original layout of *Ala* was defined as a symmetrical swept wing, spanning 96 in. and measuring 47.6 in. from nose to trailing tip. The quarter-chord of the wing is swept back 35°, $\Lambda_{w,c/4}$. On the extreme outboard trailing edge of the wing of the wing are the elevators (*1.875"x11.25"*), and immediately inboard of the elevators were the ailerons (1.875"x11.25"). [4] The nose of *Ala* was used as the reference point for all measurements. Figure 1 shows a computer-generated view of the original design. Note that the original layout did not include any vertical surfaces therefore remaining a "pure" flying wing. Figure 2 shows a computer-generated view of the final design, which included winglets at the tips. Later sections will discuss the reasoning for adding winglets to the original design. Figure 3 shows a snapshot of the final plane with *The Tailless Wonders*. The computer-generated models were created using CATIA.[4]

In order to ease the analysis process, the author created a MATLAB interface that automated the process of analyzing the stability and controllability of the plane. From the analysis of the results obtained from the MATLAB interface it was learned that the original layout would not be laterally stable and further analysis was conducted to produce reasonable levels of lateral stability considering the impossibility of using augmented flight controls. The final analysis yielded implementation of the original layout with winglets. The dimensions of the winglets were: root chord equal to the tip chord of the wings, 12 in., the tip chord of 7.2 in., semi-span of 9.8 inches and a leading edge swept 40°, $\Lambda_{LE,v}$. The consequent sections will analyze the longitudinal and lateral static and dynamic stability analysis for flying wings and will discuss in more detail the reasoning behind the need for winglets to improve the lateral stability when augmented flight controls are not possible.

This paper is divided in seven sections. The first section gives an introduction to stability. The second and third section deal with the static and dynamic stability of Ala. The fourth section presents the results for the longitudinal dynamic stability. The analysis of the dynamic lateral stability is presented in the fifth section. The analysis of the results for the lateral dynamic stability are discussed in the sixth section. Conclusions and future work are presented in sections eight and nineth.

Section I: Introduction to Ala's Stability

Ala's stability analysis was divided into static stability and dynamic stability. An airplane is considered to be statically stable if: *the forces and moments on the body caused by a disturbance tend initially to return the body toward its equilibrium position.*[1] An airplane is dynamically stable if: *out of its own accord, it eventually returns to and remains at its equilibrium position over a period of time.*[1] In order to simplify the stability and control analysis the xyz orthogonal axis system fixed relative to the airplane is used. For this system the x-axis is along the fuselage, the y-axis is along the starboard wing perpendicular to the x-axis, and the z-axis is directed downward, perpendicular to the xy-plane. In order to have a trimmed (or equilibrium) flight the moments about the center of gravity of the plane, X_{cg} must be zero. The sign convention for the direction of the moments along each of the three axes is that of the right hand rule with the thumb pointing away from the center of gravity where all the three axes meet. The stability modes associated with the x-axis, y-axis and z-axis are named lateral, longitudinal, and directional stability, respectively[1]. For example, for the longitudinal

stability, a positive moment causes a nose-up movement of the plane.

The controllability of the airplane relates the ease of the airplane changing from its original trimmed position to a different one (i.e.: maneuverability). Stability and control about all three axes is usually a necessity in the design of conventional planes, but due to the complexity and the time involved in the analysis of all three axes, the analysis was limited to the y-axis and x-axis (longitudinal and lateral stability).

Section II: Static Stability Criteria for Longitudinal Stability

The necessary criteria for longitudinal balance and static stability is that $C_{M,0}$, the moment coefficient of the airplane at zero angle of attack, (α_0), must be positive, so after a disturbance the initial tendency of the airplane will be to return to its equilibrium position. The second criteria is that $\partial C_{M,cg} / \partial \alpha_a$, the moment coefficient of the airplane with respect to its angle of attack (also detonated as $C_{M,\alpha}$), must be negative such that an equilibrium or trim angle of attack at which the moments about the center of gravity are zero can be achieved. [1] For such a configuration after a wind disturbance on a conventional aircraft, the horizontal tail counteracts the moment generated by the wing. The result is that, after the airplane is disturbed by a wind gust producing a pitching upward moment, the tail creates a negative moment about the center of gravity tending to pitch the nose downward. When the wind disturbance produces a pitching downward moment, the tail produces a positive moment that tends to pitch the nose up. Figure 4 shows the static stability behavior for a conventional airplane. However, *Ala* has no tail to provide longitudinal static stability, and therefore the means for static stability must be within the wing alone. Therefore the choice of the airfoil to be used was of critical importance. Cambered airfoils, although having high lift capabilities, could not be used for *Ala* due to its inherent negative $C_{M,0}$. For most flying wings, longitudinal stability is achieved through aerodynamic means (reflex airfoils) and/or geometric twist (changing of local incidence angle with change in span). [2] Both geometric twisting and reflex airfoils increase the complexity of both analysis and construction, but geometric twist is far simpler and lends itself to manufacturing easier than aerodynamic twist, so it was decided that *Ala* would incorporate only the former along with symmetric airfoils in order to satisfy the necessary criteria for static stability[4]. The airfoils chosen were NACA 65_3-0018 for the root and NACA 65_1-0012 for the tip. The wingtip camber lines were set at -4° angle of attack relative to the root camber line. The geometric twist of the wing tip generated, fulfilled the required criteria for static stability by inducing a slightly positive moment on the entire wing hence producing $C_{M,0}$=0.039 and $C_{M,\alpha}$=-0.00719 per degree which satisfied the criteria for static stability. The lift coefficient at zero angle of attack was $C_{L,0}$=-0.117, and lift curve slope was $C_{L,\alpha}$=4.119 per radian. The aerodynamic data was obtained using PMARC, a mature panel code capable of calculating inviscid flow about arbitrary bodies. [4] Figure 5 and 6 show the lift coefficient and the moment coefficient as a function of angle of attack respectively.

Recommendations for tailless airplanes call for a static margin at least 20% of the chord [2]. With this in mind, it was clearly observed that the sweep of the wing will greatly determine the location of the mean aerodynamic center, X_{ac}, and to a smaller extent the location of the center of gravity. The static margin is a measure of the static stability of the airplane and is defined as the percentage of the mean aerodynamic chord, $\bar{c}$, that the mean aerodynamic center lies behind the center of gravity.

$$\frac{(X_{ac} - X_{cg})}{\bar{c}} 100\% \qquad (1)$$

For a statically stable airplane, the static margin needs to be positive, which means that for flying wings the center of gravity needs to be in front of the mean aerodynamic center. With the approximate location and weight of the different wing members, an automated code was created to determine the sweep's influence on the mean aerodynamic and center of gravity. The trends for mean aerodynamic center, center of gravity and static margin versus the variation of sweep angle can be seen in Figure 7. From the aerodynamics stand point of view, the less sweep is better, therefore to optimize both aerodynamics and static stability the final layout was set at 35°, with X_{ac}=1.709 ft from the nose of the airplane, and $\bar{c}$=1.361 ft. The center of gravity depended on the desired static margin. The initial design located the center of gravity at 1.3 ft from the nose of the airplane, which corresponded to a static margin of 30%. The initial large static margin gave freedom to place equipment in the equipment bay and allowed flexibility during the construction phase. In case the construction techniques would not yield the expected center of gravity value, it was easier to increase the static margin of the plane (if needed) by adding weight to the nose of the plane rather than having to decrease it's static margin by adding weight to the end of the airplane.

Moments of inertia were also output by CATIA based on the complex physical aspects of every part contained in the craft [4]:

$I_{xx} = 1714.04\ \text{in}^4 \quad I_{yy} = 591.08\ \text{in}^4$
$I_{zz} = 2290.70\ \text{in}^4 \quad I_{xz} = 0.00\ \text{in}^4$

Section III: Dynamic Longitudinal Stability Analysis

Following initial analysis MATLAB code was expanded to determine both the longitudinal and lateral dynamic stability of the plane. The small perturbation equations of motion were used to obtain the longitudinal and lateral motion equations. In general, most of the stability derivatives that govern the dynamic behavior of an aircraft are simplified so they would only include the terms that represent the greatest contribution to their final values. For the longitudinal mode, obtaining the values for the derivatives, $C_{L_{\dot{\alpha}}}$, $C_{M_{\dot{\alpha}}}$, C_{L_q} and C_{M_q} represents a distinct challenge since, in general literature, they are expressed as functions of the horizontal tail. Literature research found a complete study by Frederick Smetana that dated back to the 1970's. Smetana decoupled all the stability derivatives regarding wing, vertical and horizontal fins and fuselage contributions, providing empirical expressions for all its contributions.[5] This represented an important advance in the task of trying to accurately predict the performance of *Ala.* For the longitudinal dynamic stability and response, the perturbed longitudinal equations of motion were transformed into the Linear Time Invariant (*LTI*), matrix form. This form of the longitudinal stability can be seen below, where the u is the forward speed, α is the angle of attack, q is the pitch rate, and θ is the pitch angle:

$$\begin{bmatrix} \dot{u} \\ \dot{\alpha} \\ \dot{q} \\ \dot{\theta} \end{bmatrix} = \begin{bmatrix} X_U + X_{T_U} & X_\alpha & 0 & -g\cos\theta_1 \\ \frac{Z_U}{U_1 - Z_{\dot{\alpha}}} & \frac{Z_\alpha}{U_1 - Z_{\dot{\alpha}}} & \frac{Z_q + U_1}{U_1 - Z_{\dot{\alpha}}} & \frac{-g\sin\theta_1}{U_1 - Z_{\dot{\alpha}}} \\ M_U + M_{T_U} + \frac{Z_U M_{\dot{\alpha}}}{U_1 - Z_{\dot{\alpha}}} & M_\alpha + M_{T_\alpha} + \frac{Z_\alpha M_{\dot{\alpha}}}{U_1 - Z_{\dot{\alpha}}} & M_q + \frac{(Z_q + U_1)M_{\dot{\alpha}}}{U_1 - Z_{\dot{\alpha}}} & \frac{-gM_{\dot{\alpha}}\sin\theta_1}{U_1 - Z_{\dot{\alpha}}} \\ 0 & 0 & 1 & 0 \end{bmatrix} \begin{bmatrix} u \\ \alpha \\ q \\ \theta \end{bmatrix} + \begin{bmatrix} X_{\delta_e} \\ \frac{Z_{\delta_e}}{U_1 - Z_{\dot{\alpha}}} \\ M_{\delta_e} + \frac{Z_{\delta_e} M_{\dot{\alpha}}}{U_1 - Z_{\dot{\alpha}}} \\ 0 \end{bmatrix} [\delta_e] \quad (1)$$

Where the linearized equations of motion can be described such:

$$X_U = -\frac{\bar{q}S(C_{D_u} + 2C_{D_1})}{mU_1} \ (2) \qquad X_{T_U} = \frac{\bar{q}S(C_{T_{Xu}} + 2C_{T_{X1}})}{mU_1} \ (3)$$

$$X_\alpha = -\frac{\bar{q}S(C_{D_\alpha} + C_{L_1})}{mU_1} \ (4) \qquad X_{\delta_e} = -\frac{\bar{q}SC_{D_{\delta_e}}}{m} \ (5)$$

$$Z_U = -\frac{\bar{q}S(C_{L_u} + 2C_{L_1})}{mU_1} \ (6) \qquad Z_\alpha = -\frac{\bar{q}S(C_{L_\alpha} + C_{D_1})}{m} \ (7)$$

$$Z_{\dot{\alpha}} = -\frac{\bar{q}S\bar{c}C_{L_{\dot{\alpha}}}}{2mU1} \ (8) \qquad Z_q = -\frac{\bar{q}S\bar{c}C_{L_q}}{2mU_1} \ (9) \qquad Z_{\delta_e} = -\frac{\bar{q}SC_{L_{\delta_e}}}{m} \ (10)$$

$$M_U = \frac{\bar{q}S\bar{c}(C_{M_u} + 2C_{M_1})}{I_{yy}U_1} \ (11) \qquad M_{T_U} = \frac{\bar{q}S\bar{c}(C_{M_{Tu}} + 2C_{M_{T_1}})}{I_{yy}U_1} \ (12)$$

$$M_\alpha = \frac{\bar{q}S\bar{c}C_{M_\alpha}}{I_{yy}} \ (13) \qquad M_{T_\alpha} = \frac{\bar{q}S\bar{c}C_{M_{T\alpha}}}{I_{yy}} \ (14)$$

$$M_{\dot{\alpha}} = \frac{\bar{q}S\bar{c}^2 C_{M_{\dot{\alpha}}}}{2I_{yy}U_1} \ (15) \qquad M_q = \frac{\bar{q}S\bar{c}^2 C_{M_q}}{2I_{yy}U_1} \ (16) \qquad M_{\delta_e} = \frac{\bar{q}S\bar{c}C_{M_{\delta_e}}}{I_{yy}} \ (17)$$

Where $\bar{q}$ is the dynamic pressure at the flight condition, S is the surface area of the aircraft (hence for flying wings equal to the surface of the wing, S_w), and m is the mass of the aircraft. The longitudinal derivative coefficients are:

$$C_{L_0} = -0.117 \quad C_{M,0} = 0.039 \quad C_{L_\alpha} = 0.071923\frac{1}{\text{deg}}$$

$$C_{M_\alpha} = -0.00719\frac{1}{\text{deg}} \quad C_{D_1} = 0.01995$$

$$C_{L_1} = C_{L_0} + C_{L_\alpha}\alpha \ (18) \qquad C_{M_1} = C_{M_0} + C_{M_\alpha}\alpha \ (19)$$

$$C_{T_{X_1}} = C_{D_1} \quad (20)$$

Note that these derivatives are specified by the airfoil's and airplane's design.

$$C_{L_U} = \frac{C_{L_1}M^2}{1 - M^2} \ (21) \qquad C_{D_U} = 0 \ (22) \qquad C_{D_\alpha} = 0 \ (23)$$

$$C_{T_{XU}} = -3C_{T_{X_1}} \ (24) \qquad C_{M_U} = 0 \ (25) \qquad C_{M_{TU}} = 0 \ (26)$$

$$C_{M_{T\alpha}} = 0 \ (27) \qquad C_{L_{\dot{\alpha}}} = 2C_{L_{\alpha_h}}\eta_h \bar{V}_h \frac{d\varepsilon}{d\alpha} \ (28)$$

$$C_{M_{\dot{\alpha}}} = -C_{L_{\dot{\alpha}}}\left(\bar{X}_{ac} - \bar{X}_{cg}\right) \ (29) \qquad C_{L_q} = 2C_{L_\alpha}\left(\bar{X}_{ac} - \bar{X}_{cg}\right) \ (30)$$

$$C_{M_q} = -C_{L_q}\left|\bar{X}_{ac} - \bar{X}_{cg}\right| \ (31) \qquad C_{L_{\delta e}} = C_{L_\alpha}\frac{d\alpha}{d\varepsilon} \ (32)$$

$$C_{M_{\delta e}} = -C_{L_{\delta e}}\frac{L_e}{\bar{c}} \quad (33)$$

Equations 20 through 27 are obtained from reference 6 assuming low-speed. Note that the rate derivatives $C_{L_{\dot{\alpha}}}$ & $C_{M_{\dot{\alpha}}}$, equations 28 and 29 respectively, are a function of the horizontal tail and therefore for flying wings are equal to zero. Equations 30 and 31 represent the wing's contribution of the pitch rate derivatives and equations 32 and 33 represent the hinge derivatives.[5]

Once all the aerodynamic derivatives required to complete the longitudinal *LTI* were implemented, the MATLAB code was verified using geometric, mass, inertia, stability, and control data for a Cessna 172 [6] in order to make sure that the results obtained were correct.

Section IV: Longitudinal Dynamic Stability results

The analysis of the longitudinal dynamic stability for the flying wing is not dependent on any vertical surfaces, therefore the MATLAB results for

longitudinal stability hold for both flying wings with and without vertical surfaces. The eigenvalues for the longitudinal *LTI* matrix yielded the Phugoid mode poles of -0.0509 ± 0.4332i and the Short Period mode poles of –5.5859 ±31.7235i. Since all the poles had a negative real part it was predicted that the plane would be inherently longitudinally stable. The Phugoid Undamped Natural Frequency, ω_{n_P}, and the Damping Frequency, ζ_P, give a better understanding of the significance of the eigenvalues.[7] The Phugoid poles are underdamped with a natural frequency of ω_{n_P} = 0.4361 and a damping ratio of ζ_P = 0.1167. The Short Period poles are also under damped with a natural frequency of ω_{n_S} = 32.2115 and a damping ratio of ζ_S=0.1734. Figure 8 represents the time response for the Phugoid mode. It is observed from the trends of the figure that the Phugoid produces a slow underdamped response after the initial perturbation, as seen by the large period of 12.6292 sec. Note that the units on the Y-axis are not scaled. This is because the magnitude of the impulse cannot be controlled and this causes large amplitude as seen. The trends of period, however, are the same despite the magnitude of a given impulse. This is true for all the stability time-response plots. Figure 9 shows the time response for the Short Period mode. It can be observed that the short period produces a rapid underdamped response after the initial perturbation,as seen by the small period of 0.1981 sec. The forward speed, angle of attack, pitch rate and pitch angle are also analyzed to observe their time response after an impulse perturbation. The forward speed, *u*, time response is plotted in Figure 10, and it is seen that after a perturbation, the forward speed slowly recovers to equilibrium as predicted by its dependency on the Phugoid mode. The angle of attack time response is plotted in Figure 11, and after a perturbation, the angle of attack recovers in a short time to equilibrium as predicted by its dependency on the Short Period mode. The pitch rate, $\dot{q}$, time response is plotted in Figure 12 and it is observed to rapidly return to equilibrium after a perturbation. The pitch angle time response is plotted in Figure 13, and it can be observed that following a perturbation it slowly recovers to equilibrium as predicted by its dependency on the Phugoid mode.

Section V: Lateral Dynamic Stability Analysis

The analysis of the lateral dynamic stability for flying wings had to be closely analyzed since most of the lateral stability derivatives are a function of the vertical tail, and decoupling of wing and vertical surfaces was necessary for determining if winglets were required to attain lateral stable flight. The *LTI* form of the lateral stability can be seen below, where *v* is the side-slip velocity, *p* is the roll rate, *r* is the yaw rate, ϕ is the bank angle, and ψ is the heading angle. As in the case of the dynamic longitudinal stability analysis, most of the derivatives that govern the dynamic behavior of an aircraft are simplified such that only account for the vertical tail contribution. Again, Smetana's empirical equations for the wing's contributions to the lateral stability derivatives were used to be able to model the dynamics of the flying wing.[5] Note that in the lateral *LTI,* the forcing function vector is only a function of the aileron deflection. *Ala* did not have rudder control hence the *LTI* was modified to account for this fact

$$\begin{bmatrix} \dot{\beta} \\ \dot{p} \\ \dot{r} \\ \dot{\phi} \\ \dot{\psi} \end{bmatrix} = \begin{bmatrix} \frac{Y_\beta}{U_1} & Y_p & Y_r - U_1 & g\cos\theta_0 & 0 \\ \frac{L_\beta + A_1[N_\beta + N_{T\beta}]}{(1-A_1B_1)U_1} & \frac{L_p + A_1N_p}{1-A_1B_1} & \frac{L_r + A_1N_r}{1-A_1B_1} & 0 & 0 \\ \frac{B_1L_\beta + N_\beta + N_{T\beta}}{(1-A_1B_1)U_1} & \frac{B_1L_p + N_p}{1-A_1B_1} & \frac{B_1L_r + N_r}{1-A_1B_1} & 0 & 0 \\ 0 & 1 & \tan\theta_0 & 0 & 0 \\ 0 & 0 & \frac{1}{\cos\theta_0} & 0 & 0 \end{bmatrix} \begin{bmatrix} \beta \\ p \\ r \\ \phi \\ \psi \end{bmatrix} + \begin{bmatrix} \frac{Y_{\delta_A}}{L_{\delta_A} + A_1N_{\delta_A}} & \frac{Y_{\delta_r}}{L_{\delta_r} + A_1N_{\delta_r}} \\ \frac{1-A_1B_1}{B_1L_{\delta_A} + N_{\delta_A}} & \frac{1-A_1B_1}{B_1L_{\delta_r} + N_{\delta_r}} \\ \frac{1-A_1B_1}{0} & \frac{1-A_1B_1}{0} \\ 0 & 0 \end{bmatrix} \begin{bmatrix} \delta_A \\ \delta_r \end{bmatrix} \quad (34)$$

Where the linearized equations of motion can be described such:

$$Y_\beta = \frac{\bar{q}SC_{Y_\beta}}{m} (35) \quad Y_p = \frac{\bar{q}SbC_{Y_p}}{2mU_1} (36) \quad Y_r = \frac{\bar{q}SbC_{Y_r}}{2mU_1}$$

$$(37)\ Y_{\delta_a} = \frac{\bar{q}SC_{Y_{\delta_a}}}{m} (38)\ Y_{\delta_r} = \frac{\bar{q}SC_{Y_{\delta_r}}}{m} (39)$$

$$L_\beta = \frac{\bar{q}SbC_{l_\beta}}{I_{xx}} (40) \quad L_p = \frac{\bar{q}Sb^2C_{l_p}}{2I_{xx}U_1} (41)$$

$$L_r = \frac{\bar{q}Sb^2C_{l_r}}{2I_{xx}U_1} (42) \quad L_{\delta_a} = \frac{\bar{q}SbC_{l_{\delta_a}}}{I_{xx}} (43)$$

$$L_{\delta_r} = \frac{\bar{q}SbC_{l_{\delta_r}}}{I_{xx}} (44) \quad N_\beta = \frac{\bar{q}SbC_{n_\beta}}{I_{zz}} (45)$$

$$N_{T_\beta} = \frac{\bar{q}SbC_{n_{T\beta}}}{I_{zz}} (46) \quad N_p = \frac{\bar{q}Sb^2C_{n_p}}{2I_{zz}U_1} (47)$$

$$N_r = \frac{\bar{q}Sb^2C_{n_r}}{2I_{zz}U_1} (48) \quad N_{\delta_a} = \frac{\bar{q}SbC_{n_{\delta_a}}}{I_{zz}} (49)$$

$$N_{\delta_r} = \frac{\bar{q}SbC_{n_{\delta_r}}}{I_{zz}} (50)$$

Where *b* is the wingspan. All the lateral derivative coefficients are decoupled to account for both wing and vertical fin contributions. The subscript w denotes the wing contribution, while the subscript v denotes the

vertical surface contribution, which for this study is the winglets' contribution.

$$C_{Y_\beta} = C_{Y_{\beta,w}} + C_{Y_{\beta,v}} \quad (51)$$

$$C_{Y_{\beta,w}} = C_{L_1}{}^2 \frac{6\tan\Lambda_w \sin\Lambda_w}{\pi AR(AR+4\cos\Lambda_w)} \quad (52)$$

$$C_{Y_{\beta,v}} = -k(C_{L_\alpha})_v(1+\frac{\partial\sigma}{\partial\beta})\frac{q_v}{q}\frac{S_v}{S_w} \quad (53) \text{ or}$$

$$C_{Y_{\beta,v}} = -C_{L_{\alpha,v}}\frac{q_v}{q}\frac{S_v}{S_w}$$

Where AR is the aspect ration of the wing, Λ_w is the sweep of the wing, k is an empirical factor obtained from reference 5, $(C_{L_\alpha})_v$ is the three dimensional lift curve slope of the vertical fin, $(1+\frac{\partial\sigma}{\partial\beta})$ is the sidewash, $\frac{q_v}{q}$ is the dynamic pressure ratio and $\frac{S_v}{S_w}$ is the surface area ratio.

$$C_{Y_p} = C_{Y_{p,w}} + C_{Y_{p,v}} \quad (54)$$

$$C_{Y_{p,w}} = C_{L_1}\left(\frac{AR+\cos\Lambda_w}{AR+4\cos\Lambda_w}\tan\Lambda_w + \frac{1}{AR}\right) \quad (55)$$

$$C_{Y_{p,v}} = -2C_{L_{\alpha,v}}\frac{z_v}{b}\frac{q_v}{q}\frac{S_v}{S_w} \quad (56)$$

Where z_v is the height of the vertical tail center of pressure above the longitudinal axis.

$$C_{Y_r} = C_{Y_{r,w}} + C_{Y_{r,v}} \quad (57)$$

$$C_{Y_{r,w}} = 0.143C_{L_1} - 0.05 \quad (58) \qquad C_{Y_{r,v}} = -2\frac{l_v}{b}C_{Y_{\beta,v}} \quad (59)$$

where l_v is the moment arm from the center of pressure of the vertical tail to the center of gravity of the aircraft.

$$C_{Y_{\delta_a}} = 0 \quad (60) \qquad C_{Y_{\delta_r}} = C_{L_{\alpha,v}}\tau\frac{S_v}{S_w} = 0 \quad (61)$$

Equation 60 is an approximation for light aircraft[6], and equation 61 is due to the fact that Ala lacks of rudder control.

$$C_{l_\beta} = C_{l_{\beta,w}} + C_{l_{\beta,v}} \quad (62)$$

$$C_{l_{\beta,w}} = C_{L_1}\left(-k\frac{(0.71\lambda+0.29)}{AR\lambda} + 0.05\right) \quad (63)$$

$$C_{l_{\beta,v}} = -C_{L\alpha,v}\left(1-\frac{\partial\sigma}{\partial\beta}\right)\frac{S_v}{S_w}\frac{z_v}{b}\frac{q_v}{q} \quad (64) \text{ or } C_{l_{\beta,v}} = -a_v\frac{S_v}{S_w}\frac{z_v}{b}\frac{q_v}{q}$$

Where a_v is the lift curve slope of the vertical tail and is determined using the effective aspect ratio $Ae = 1.55\frac{b_v^2}{S_v}$ and reference 5 to obtain a_v and λ is the wing taper ratio of the wing.

$$C_{l_p} = C_{l_{p,w}} + C_{l_{p,v}} \quad (65)$$

$$C_{L_{p,w}} = C_{L_{p,a0}} - \frac{1}{8}\frac{C_{L_1}{}^2}{\pi AR\cos^2\Lambda_w}\left(1+2\sin^2\Lambda_w\frac{AR+2\cos\Lambda_w}{AR+4\cos\Lambda_w}\right) - \frac{1}{8}C_{D_1} \quad (66)$$

$$C_{L_{p,v}} = 2\left(\frac{z_v}{b}\right)^2 C_{Y_{\beta,v}} \quad (67) \text{ or } C_{L_{p,v}} = -2C_{L\alpha,v}\left(\frac{z_v}{b}\right)^2\frac{q_v}{q}\frac{S_v}{S}$$

Where $C_{L_{p,a0}}$ is extracted from analytical graphs in reference 5.

$$C_{l_r} = C_{l_{r,w}} + C_{l_{r,v}} \quad (68) \qquad C_{l_{r,w}} = \frac{C_{L_1}}{3} \quad (69)$$

$$C_{l_{r,v}} = -2\frac{l_v z_v}{b^2}C_{Y_{\beta,v}} \quad (70) \text{ or } C_{l_{r,v}} = 2C_{L\alpha,v}\frac{l_v z_v}{b^2}\frac{S_v}{S_w}\frac{q_v}{q}$$

$$C_{l_{\delta_a}} = \frac{2C_{L_\alpha}\tau}{S_v S_w}\int_a^b cydy \quad (71)$$

$$C_{l_{\delta_r}} = a_v\tau\frac{S_v}{S_w}\frac{z_v}{b} = 0 \quad (72) \text{ since no rudder on } Ala$$

$$C_{n_\beta} = C_{n_{\beta,w}} + C_{n_{\beta,v}} \quad (73)$$

$$C_{n_{\beta,w}} = C_{L_1}{}^2\left(\frac{1}{4\pi AR} - \frac{\tan\Lambda_w}{\pi AR(AR+4\cos\Lambda_w)}\right.$$
$$\left.(\cos\Lambda_w - \frac{AR}{2} - \frac{AR^2}{8\cos\Lambda_w}) + 6\frac{\bar{x}}{c}\frac{\sin\Lambda_w}{AR}\right) \quad (74)$$

$$C_{n_{\beta,v}} = C_{L_{\alpha_v}}\left(1-\frac{\partial\sigma}{\partial\beta}\right)\frac{S_v}{S_w}\frac{z_v}{b}\frac{q_v}{q} \quad (75) \text{ or } C_{n_{\beta,v}} = a_v\frac{S_v}{S_w}\frac{z_v}{b}\frac{q_v}{q}$$

Where $\bar{x}$ is the longitudinal distance rearward from the X_{cg} to X_{ac}, and τ is an empirical parameter obtained from reference 5.

$$C_{n_p} = C_{n_{p,w}} + C_{n_{p,v}} \quad (76)$$

$$C_{n_{p,w}} = C_{L_1}\frac{AR+4}{AR+4\cos\Lambda_w}\left(1+6(1+\frac{\cos\Lambda_w}{AR})\frac{\tan^2\Lambda_w}{12}\right)\left(\frac{C_{n_p}}{C_L}\right)_{\Lambda_w=0} \quad (77)$$

$$C_{n_{p,v}} = 2C_{L_{\alpha_v}}\frac{z_v l_v}{b^2}\frac{q_v}{q}\frac{S_v}{S_w} \quad (78)$$

where $\left(\frac{C_{n_p}}{C_L}\right)_{\Lambda_w=0}$ is an empirical parameter obtained from reference 5.

$$C_{n_r} = C_{n_{r,w}} + C_{n_{r,v}} \quad (79)$$

$$C_{n_{r,w}} = -0.33\left(\frac{1+3\lambda}{2+2\lambda}\right)C_{D_0} - 0.02\left(1-\frac{AR-6}{13}-\frac{1-\lambda}{2.5}\right)C_{L_1}{}^2 \quad (80)$$

$$C_{n_{r,v}} = -2C_{L_{\alpha_v}}\left(\frac{l_v}{b}\right)^2\frac{q_v}{q}\frac{S_v}{S_w} \quad (81) \qquad C_{n_{\delta_a}} = 2kC_{L_1}C_{l_{\delta_a}} \quad (82)$$

where k obtained from reference 5 and $C_{n_{\delta_r}} = 0_{L_{\delta_a}}$ (83) since no rudder

Note that all the lateral stability derivatives have been decoupled into wing and vertical tail contributions. This predicted if the flying wing would be stable without adding winglets

Section VI: Lateral Dynamic Stability Results

For the initial part of the lateral dynamic analysis, only the wing contribution to the lateral stability derivatives was used. The vertical tail contribution was set equal to zero in order to determine if the plane

would be stable without vertical fins. The eigenvalues for the lateral *LTI* matrix produced Dutch Roll poles of 0.0704±1.0210i, a spiral pole of –0.0879 and a roll pole of –7.5231. The real part of Dutch Roll poles was positive, predicting an inherently laterally instable airplane. For the Dutch Roll mode the time to half amplitude was 9.84 sec. and the period 6.15 sec. Such amplitude and period trends were too slow for a desirable Dutch Roll mode. [6] The Dutch Roll Damping Frequency, was ζ_D =0.068, and the Undamped Dutch Natural Frequency was ω_{n_D} = 1.0235 rad/sec. The instability predicted by the sign of the real part of the Dutch Roll poles was also corroborated by the necessary criteria for lateral-directional stability which required C_{l_β} to be negative and with magnitude of half of C_{n_β}. [8] The MATLAB interface predicted that for the original configuration, with no winglets, C_{l_β} =-0.0115 and C_{n_β} =-1.2654 e-4 which did not satisfy the second criteria for lateral-direction stability.

In order to improve such instability it was decided to focus on improving the Dutch Roll poles by studying the possibility of increasing both the Dutch Roll Undamped Natural Frequency and Damping Ratio. According to MIL-F-8785, all type of airplanes can be classified onto four classes[9]:

- Class I: Small, light airplanes.
- Class II: Medium weight, low-to-medium maneuverability airplanes.
- Class III: Large, heavy, low-to-medium maneuverability airplanes.
- Class IV: High maneuverability airplanes.

Each one of the four classes can be divided in specific flight regimes, denoted as Flight Phase Categories. According to MIL-F-8785 definitions *Ala* qualified on the Flight Phase Category A for reconnaissance regime, and the Class I type for small light airplanes. Under these specifications the minimum requirements for a Class I airplane with flight phase A were that ζ_D =0.19, and ω_{n_D} = 1.0 rad/sec.[6] It is known that vertical surfaces are important, if not the sole contribution, to lateral stability as seen by the lateral derivatives coefficients in equations 53 through 82. Using the specified requirements for minimum Dutch Roll Undamped Natural Frequency and Damping Ratio for a Class I airplane under a Flight Phase Category A, analysis was started by varying the effective surface area of both winglet relative to the percentage of the total wing area, S_W, the leading edge sweep of the winglet, $\Lambda_{LE,v}$, and the winglet's taper ratio, λ_v. The effective surface area of the winglet was varied up to 30 % of the total S_W. The sweep of the winglet was varied up to 40° in increments of 10 °, and the taper ratio was varied from 0.2 to 0.8 in increments of 0.2. The analysis yielded an sizable amount of information in the form of graphs and empirical data describing the influence of vertical winglet size and shape on the lateral dynamic stability for a flying wing.

Figures 14 through 17 show the trends for Dutch Roll damping ratio as a function of the winglet area, with variation of winglet leading edge sweep and winglet's taper ratio. It is observed that for a fixed leading edge sweep ($\Lambda_{LE,v}$) of 10°, 20°, 30°and 40° (see figures 14 through 17 respectively) the Dutch Roll damping ratio increases with decreasing winglet taper ratio keeping the same percentage of total wing area, hence achieving the required damping ratio with a smaller winglet. For a fixed Dutch Roll damping ratio, the required winglet area increases with increase of winglet taper ratio. Note that the total winglet area, which is defined as a percentage of the total wing area, accounts for the area of both winglets.

Figures 18 through 21 show the behavior of Dutch Roll Undamped Natural frequency as a function of the winglet area, with variation of winglet leading edge sweep and winglet taper ratio. It is observed that for a fixed winglet leading edge sweep the Dutch Roll natural frequency increases with decreasing winglet taper ratio, while holding the winglet area constant, hence achieving the required Dutch Roll natural frequency with smaller winglet sizes. For a fixed Dutch Roll natural frequency the required winglet area increases with increase of winglet taper ratio.

Figures 22 through 25 show the behavior of longitudinal mean aerodynamic center of the winglet as a function of the winglet area, with variation of winglet leading edge sweep and winglet taper ratio .It is observed that for a fixed winglet leading edge sweep the mean aerodynamic center increases linearly with increasing winglet area and decreasing winglet taper ratio while holding the winglet area constant. This causes larger bigger mean aerodynamic center for a smaller winglet taper ratio, which ultimately means an increase of the effective moment arm, l_v, which is a direct measurement of the lateral dynamic stability as seen on equations 59, 70, 78 and 81. For a fixed mean aerodynamic center the required winglet area increases with increasing winglet taper ratio. Figures 22 and 23 show a deviation from this linear behavior. For the range of winglet areas of 5% to 12.5% of the total wing area for Figures 22 and 23 it can be seen that for a winglet taper ratio of 0.2 it generates smaller mean aerodynamic values than those for a winglet taper ratio of 0.4 for the same range of winglet area.

Figures 26 through 29 show the behavior of vertical coordinate of the mean aerodynamic center of the winglet, z_v, as a function of the winglet area, with variation of winglet leading edge sweep and winglet's

taper ratio. It is observed that for a fixed winglet leading edge sweep, the vertical coordinate of the mean aerodynamic center increases linearly with increasing winglet area and decreasing winglet taper ratio. This is an important trend since the vertical coordinate of the mean aerodynamic center of the winglet is a direct measurement of the lateral dynamic stability as seen in equations 56, 64, 67, 70, 72, 75 and 78. For a fixed z_v the required winglet area increases with increase of winglet taper ratio.

With these results the MATLAB interface is used to compare the dynamic lateral responses for different Dutch Roll damping ratio. Figures 30 through 35 show the Dutch Roll, side-slip velocity, roll rate, yaw rate, bank angle, and heading angle respectively following an impulse perturbation for three cases: no winglets, winglets for ζ_D= 0.19, which is the minimum requirement for Class I airplanes, and winglets for ζ_D=0.25. Figures 30 through 32 show that the Dutch Roll mode, the sideslip velocity and the roll rate for the winglet cases come quickly to an equilibrium while the no-winglet case shows an unstable oscillation for the sideslip velocity and the roll rate (Figures 31 and 32), and a extremely slow stable oscillation to equilibrium for the Dutch Roll.

Figure 33 shows the yaw rate response following an impulse perturbation for three cases. All three cases show an unstable behavior. For the winglet cases, an underdamped motion that tries to settle to a steady state value is seen. The response retains this behavior as long as the damping remains small following the initial instants after an impulse perturbation. As soon as the damping becomes larger, therefore diminishing the oscillation of the yaw rate, the response becomes overdamped and departs to an exponential unstable mode. For the no-winglet case the yaw rate response after an impulse perturbation is an increasing unstable oscillatory motion. Figure 34 shows the bank angle response following an impulse perturbation for the three described cases. It is also seen that the winglet cases follow an exponential unstable mode after a brief overdamped motion. Figure 35 shows the heading angle response following an impulse perturbation for the three described cases. For the winglet cases, a critically damped motion on the first half-second is followed by an exponential unstable departure. For the no-winglet case the heading angle response after an impulse perturbation is an increasing unstable oscillatory motion.

The unstable behavior of the yaw rate, bank and heading angle for the winglet case can be explained by the trends of the poles of the lateral *LTI* matrix. For the winglet case of damping ratio of 0.19, the Dutch Roll poles are –1.3728±7.0871i, a spiral pole of 0.0645 and a roll pole of –7.6239. The real part of the Dutch Roll poles is negative predicting an inherently laterally dynamic stable airplane. The Dutch Roll response for the winglet case is much faster than that of the no-winglet case with time to half amplitude of 0.5 sec. and a period 0.88 sec. This response is much appropriate for a lateral-dynamic stable airplane. The Undamped Dutch Natural Frequency is ω_{n_D} = 7.2189 rad/sec. The criteria for lateral-directional stability is also satisfied by giving C_{l_β}=-0.0258 and C_{n_β}=0.049. The slightly positive spiral pole in addition to the lack of rudder to control the attitude of the airplane, produces the unstable departure of the yaw rate, bank and heading angle after a perturbation.

In order to have a better understanding of the behavior of the dynamic lateral stability for different Dutch damping ratios, three cases are further analyzed: winglets for ζ_D=0.15, smaller than the minimum requirement, winglets for ζ_D=0.19 and winglets for ζ_D=0.25, above the minimum requirement. Figures 36 and 37 show the Dutch Roll and sideslip velocity response after an impulse perturbation for the three winglet cases. It is observed that the amplitude and period decrease while the frequency increases with increasing Dutch damping ratio. Figure shows the roll rate response after an impulse perturbation for the three winglet cases, and as previously mentioned it is observed that the overdamped motion of response gets augmented with increasing winglet area. Figures 39 through 40 show the response after an impulse perturbation for the yaw rate, bank and heading angle respectively for the three winglet cases. The instability modes of the responses get slightly diminished as the damping ratio is increased.

The data obtained from the iterations yielded a series of different winglet planforms that meet or exceed the minimum required Dutch damping ratios for lateral-dynamic stably flight. Figure 42 shows a sample of the winglet planforms generated. At this point, since all presented planforms meet or exceed the minimum requirements [9] the choice for the desired winglet was based on what was most aesthetically pleasing for the members of the group.

The results yielded that winglet with the following dimensions be used: root chord equal to the tip chord of the wings, 12 inches, tip chord of 7.2 inches, semi-span of 9.6 in. and with a leading edge swept 40°. This would produce a Dutch damping ratio of ζ_D=0.19.

Section VII: Conclusions

The actual performances of the flying wing exceed the MATLAB's predictions. The airplane accomplished numerous acrobatic maneuvers such loops, barrel rolls, inverted flight and quasi-hammerheads. It has been shown that by decoupling the longitudinal and lateral

stability derivatives into their wing and vertical tail components, and subsequent analysis of the *LTI*, one can achieve longitudinal and lateral stability for unconventional airplanes, such flying wings, without the aid of augmented systems.

It is also shown that by selecting the correct winglet parameters, leading edge sweep, taper ratio and winglet area, the effective moment arm, l_v, and the vertical coordinate of the mean aerodynamic center of the winglet, z_v, a model can be constructed so the desired lateral stability characteristics for an airplane can be achieved.

Section VIII: Future Work

Future work include the refinement of all the codes to convert it into a Windows based interface. Currently working in introducing fuselage contributions to be able to have a better model, and ideally if time and resources permit it, wind tunnel analysis to check empirical results for lateral stability derivatives.

Acknowledgements

I would like to acknowledge all the members of *The Tailless Wonders*, for their wonderful work throughout the two semesters, Fall 1998 and Spring 1999 that concluded with the magnificent flight of our plane on April 20th 1999. Dr. Walter Eversman for his help and guidance on the area of stability and control. Dr. Frederick Smetana for making available the decoupled stability derivatives that allowed to obtain good estimates for the lateral stability derivatives for "pure" flying wings. The author is grateful to the reviewers for their valuable comments, which improved the quality of the paper.

References

[1] Anderson, John D., "Introduction to Flight", McGraw-Hill, Inc., New York, 1989.

[2] Nickel, Karl, and Michael Wohlfahrt, "Tailless Aircraft – In Theory and Practice", American Institute of Aeronautics and Astronautics, Inc., Washington, DC, 1994.

[3] Eversman, Walter, "Project Snapshot: Request for Proposal", Senior Design Guidelines, University of Missouri-Rolla, Dept. of Mechanical and Aerospace Engineering and Engineering Mechanics, University of Missouri-Rolla, Rolla, MO, August 1998.

[4] DeBons, C. B., Esteban, S., Gray, K. P., McDonald, R. A., Skoch, C. R. and Szyhowski, A. M., "The Tailless Wonders, Project Ala Voladora: A Proposal. ", Senior Design Report, Dept. of Mechanical and Aerospace Engineering and Engineering Mechanics, University of Missouri-Rolla, Rolla, MO, May 1999.

[5] Smetana, Frederick O, Delbert C. Summey, and W. Donald Johnson, "Riding and Handling Qualities of Light Aircraft – A Review and Analysis", NASA CR-1975, Washington, D.C., March 1972

[6] Roskam, Jan, "Airplane Flights and Automatic Flight Controls", Volume I and Volume II, DARcorporation, Kansas City, 1995.

[7] Etkin, Bernard, and Lloyd Duff Reid, "Dynamics of Flight – Stability and Control", John Wiley & Sons, Inc., 1996

[8] Raymer, Daniel P., "Aircraft Design: A Conceptual Approach", American Institute of Aeronautics and Astronautics, Inc., Washington, DC, 1992.

[9] Anon.; "MIL-F-8785C, Military Specification Flying Qualities of Piloted Airplanes"; November 5, 1980; Air Force Flight Dynamics Laboratory, WPAFB, Dayton, Ohio.

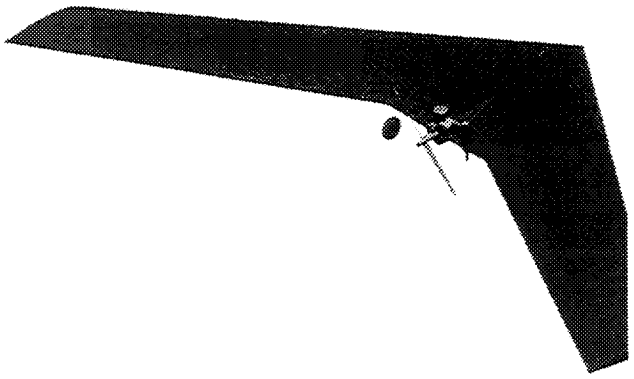

Figure1 Ala with no winglets

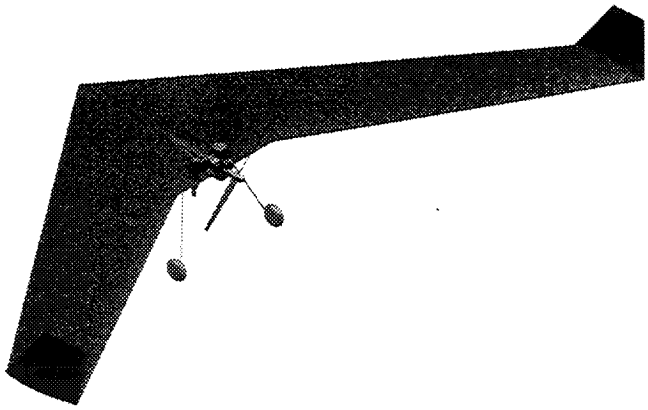

Fig. 2 Ala Voladora with winglets.

Fig. 3 Ala Voladora and the Tailless Wonders

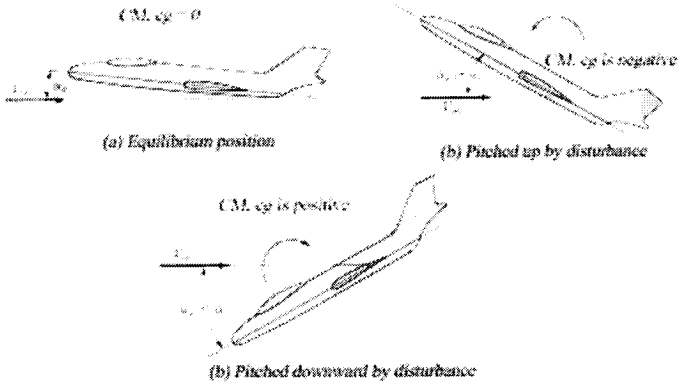

Fig. 4 Static Stability for Conventional Aircraft

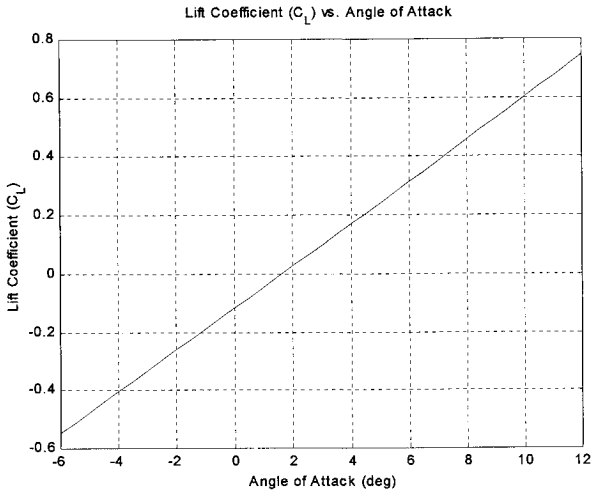

Fig. 5 Lift Coefficient vs.Angle of Attack

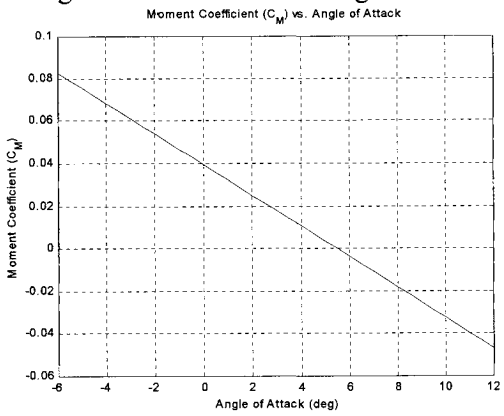

Fig. 6 Moment Coefficient vs. Angle of Attack

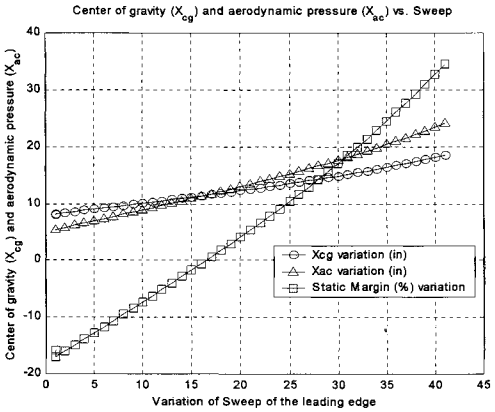

Fig. 7 X_{cg} and X_{ac} vs Angle of Attack

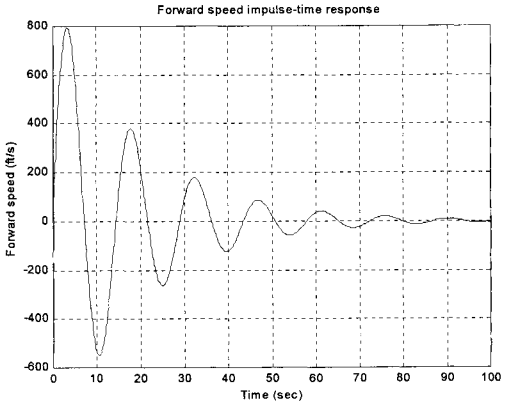

Fig. 10 Forward Speed Response After an Impulse Perturbation

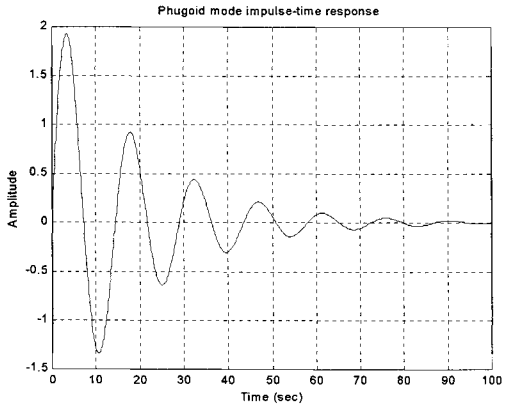

Fig. 8 Phugoid Response After an Impulse Perturbation

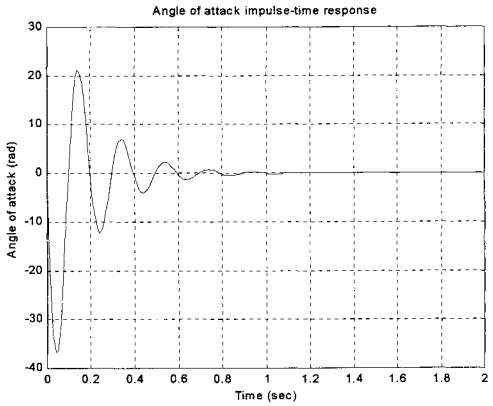

Fig. 11 AoA Response After an Impulse Perturbation

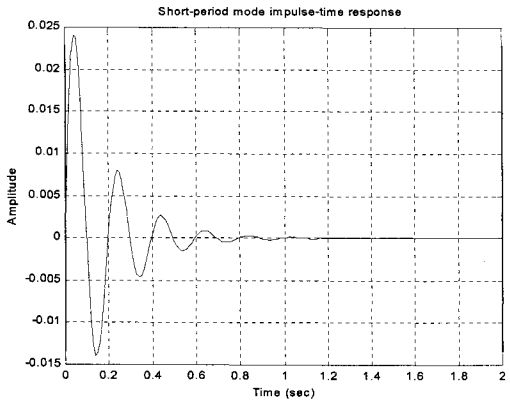

Fig. 9 Short-Period Response After an Impulse Perturbation

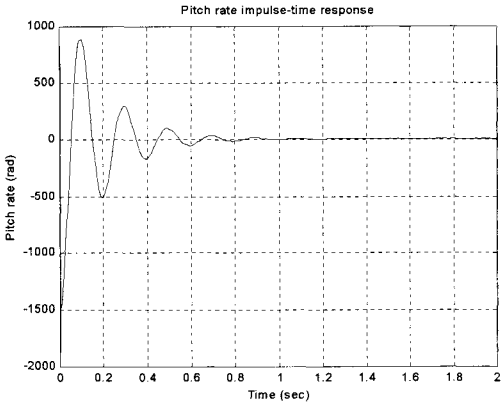

Fig. 12 Pitch Rate Response After an Impulse Perturbation

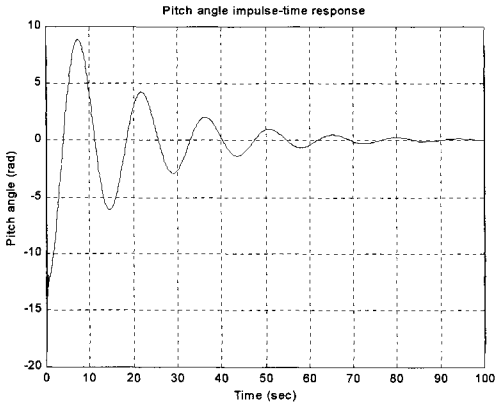

Fig. 13 Pitch Angle Response After an Impulse Perturbation

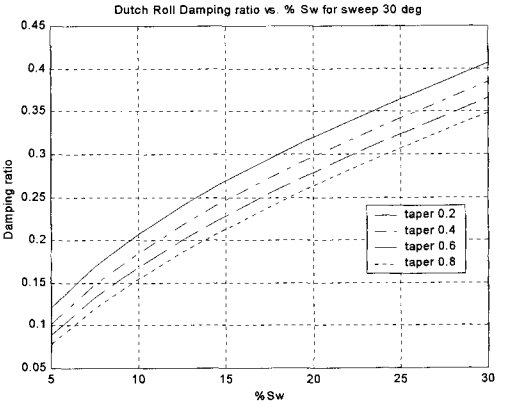

Fig. 16 ζ_D vs. Winglets' Area for $\Lambda_{v,L.E.}$ =30°

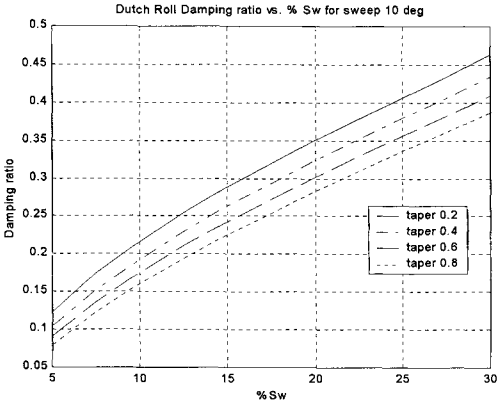

Fig. 14 ζ_D vs. Winglets' Area for $\Lambda_{v,L.E.}$ =10°

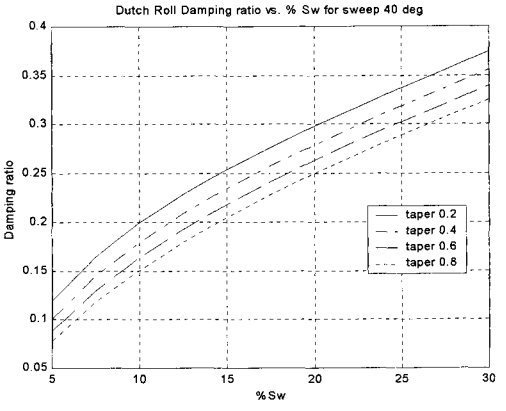

Fig. 17 ζ_D vs. Winglets' Area for $\Lambda_{v,L.E.}$ =40°

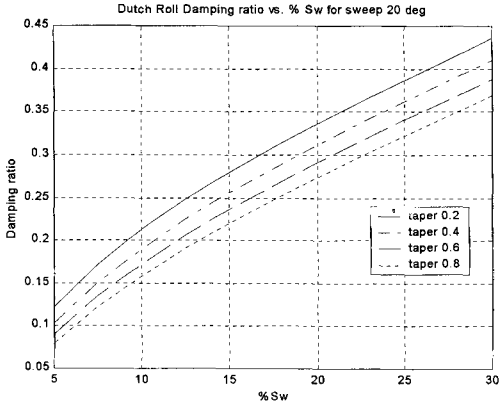

Fig. 15 ζ_D vs. Winglets' Area for $\Lambda_{v,L.E.}$ =20°

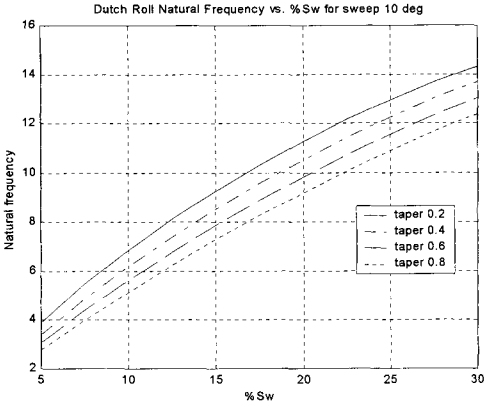

Fig. 18 ω_{Dn} vs. Winglets' Area for $\Lambda_{v,L.E.}$ =10°

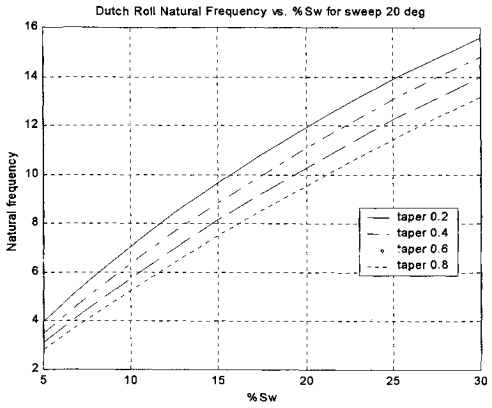

Fig. 19 ω_{Dn} vs. Winglets' Area for $\Lambda_{v,L.E.}$ =20°

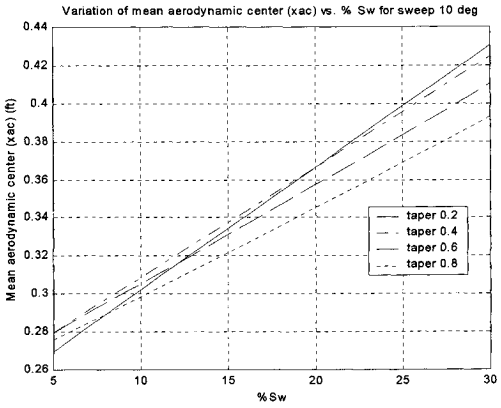

Fig. 22 X_{ac} vs. Winglets' Area for $\Lambda_{v,L.E.}$ =10°

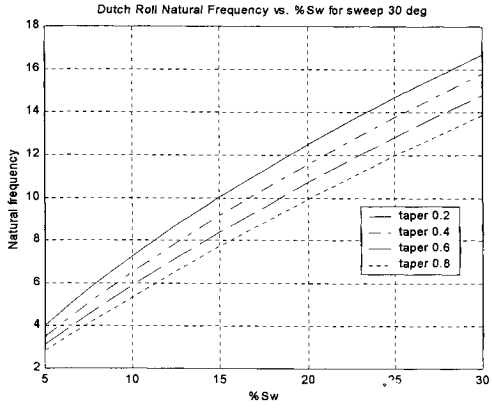

Fig. 20 ω_{Dn} vs. Winglets' Area for $\Lambda_{v,L.E.}$ =30°

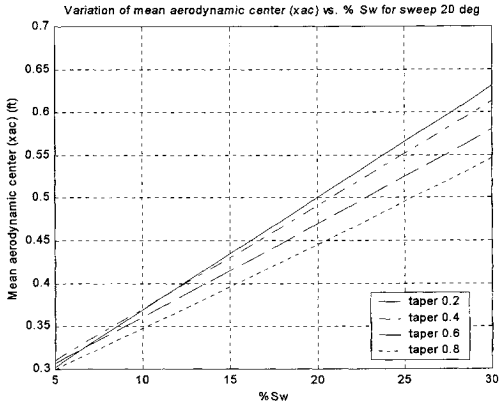

Fig. 23 X_{ac} vs. Winglets' Area for $\Lambda_{v,L.E.}$ =20°

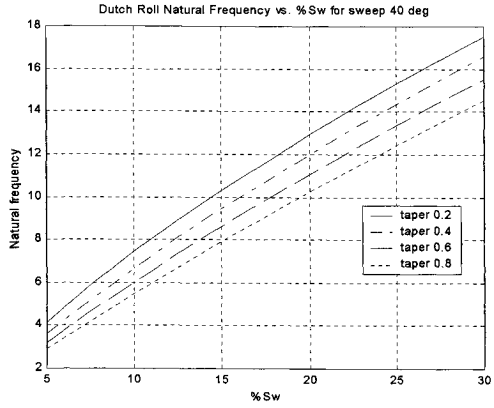

Fig. 21 ω_{Dn} vs. Winglets' Area for $\Lambda_{v,L.E.}$ =40°

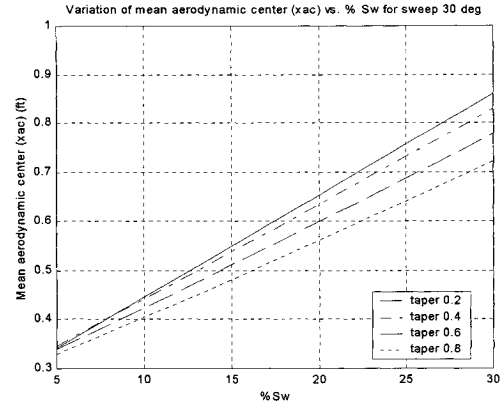

Fig. 24 X_{ac} vs. Winglets' Area for $\Lambda_{v,L.E.}$ =30°

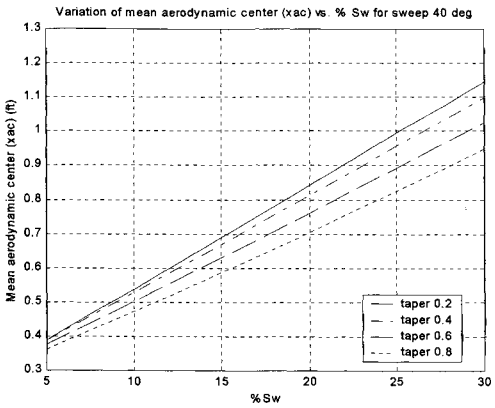

Fig. 25 X_{ac} vs. Winglets' Area for $\Lambda_{v,L.E.}$ =40

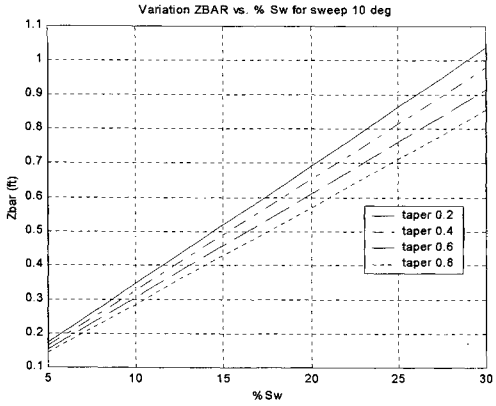

Fig. 26 $\bar{z}$ vs. Winglets' Area for $\Lambda_{v,L.E.}$ =10°

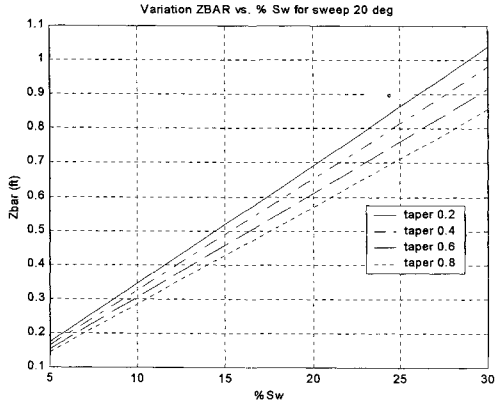

Fig. 27 $\bar{z}$ vs. Winglets' Area for $\Lambda_{v,L.E.}$ =20°

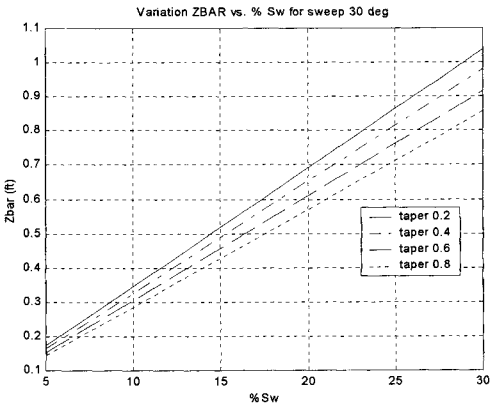

Fig. 28 $\bar{z}$ vs. Winglets' Area for $\Lambda_{v,L.E.}$ =30°

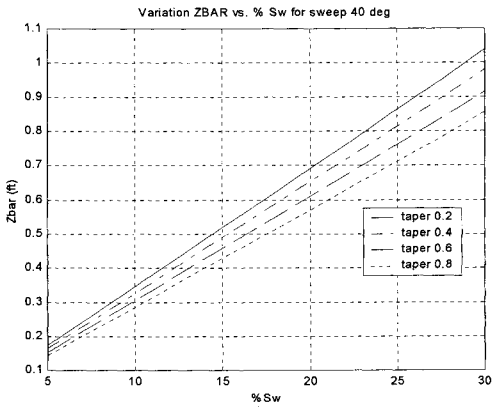

Fig. 29 $\bar{z}$ vs. Winglets' Area for $\Lambda_{v,L.E.}$ =40°

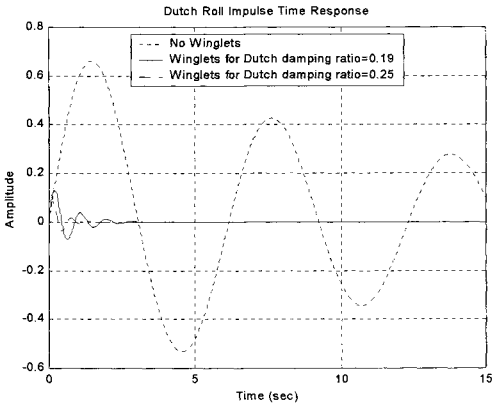

Fig. 30 Dutch Roll Response After an Impulse Perturbation

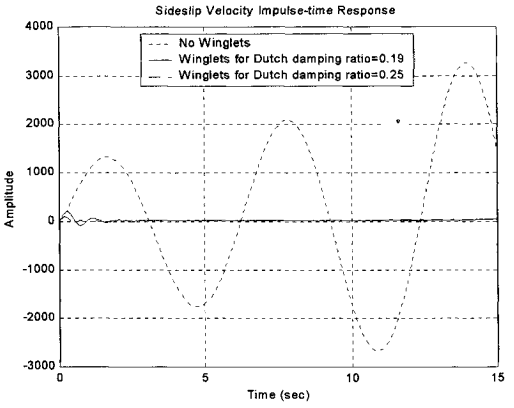

Fig. 31 Sideslip Velocity Response After an Impulse Perturbation

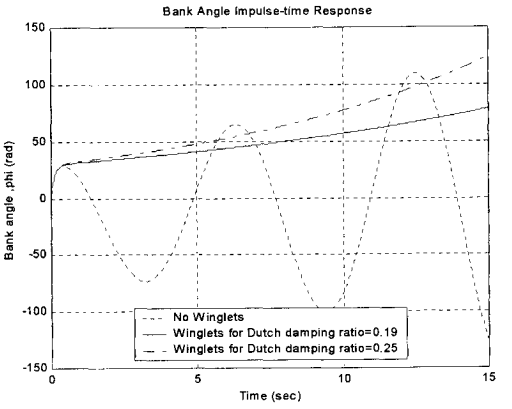

Fig. 34 Bank Angle Response After an Impulse Perturbation

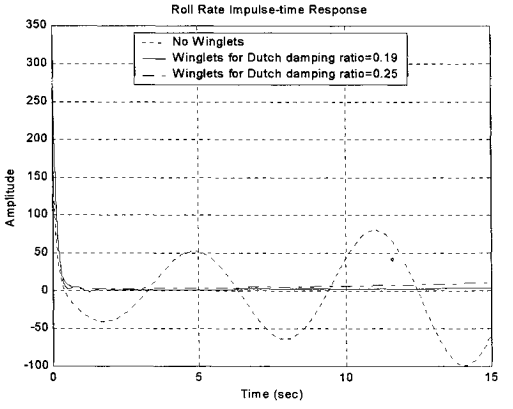

Fig. 32 Roll Rate Response After an Impulse Perturbation

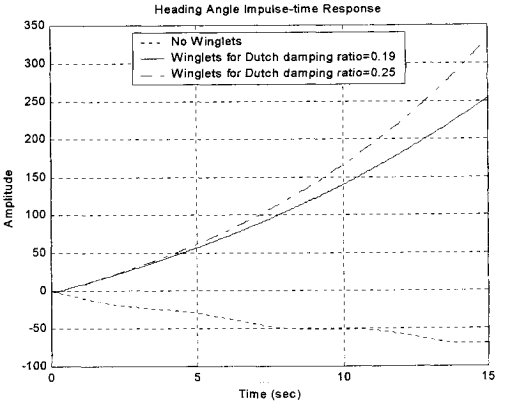

Fig. 35 Heading Angle Response After an Impulse Perturbation

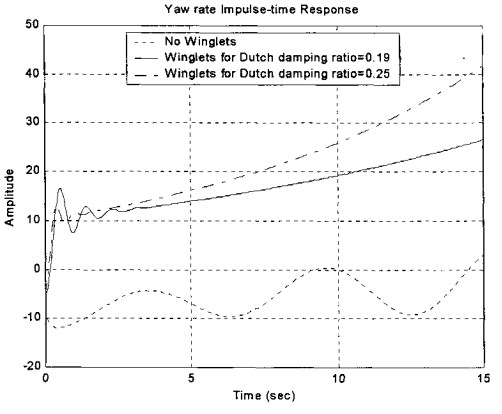

Fig. 33 Yaw Rate Response After an Impulse Perturbation

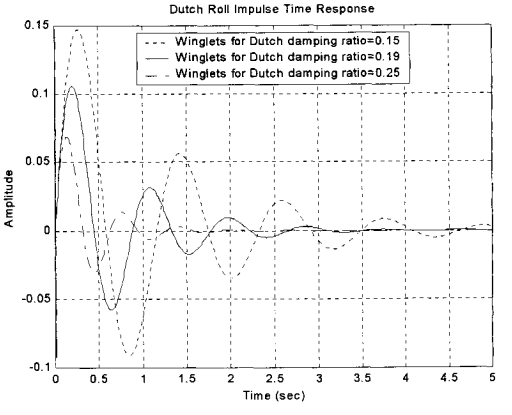

Fig. 36 Dutch Roll Response After an Impulse Perturbation

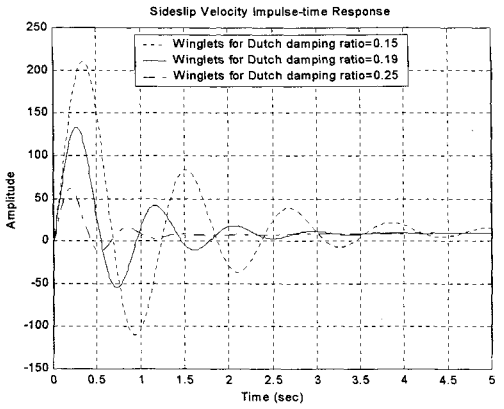

Fig. 37 Sideslip Velocity Response After an Impulse Perturbation

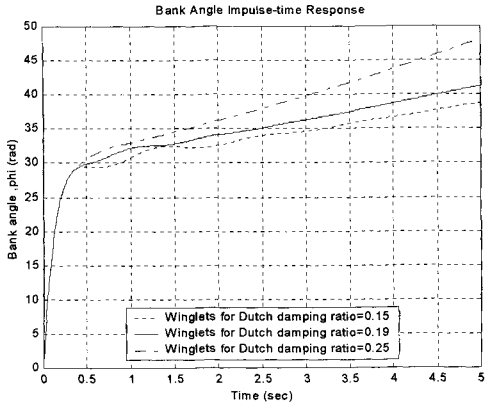

Fig. 40 Bank Angle Response After an Impulse Perturbation

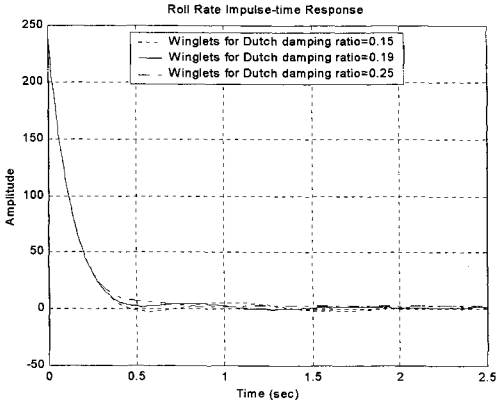

Fig. 38 Roll Rate Response After an Impulse Perturbation

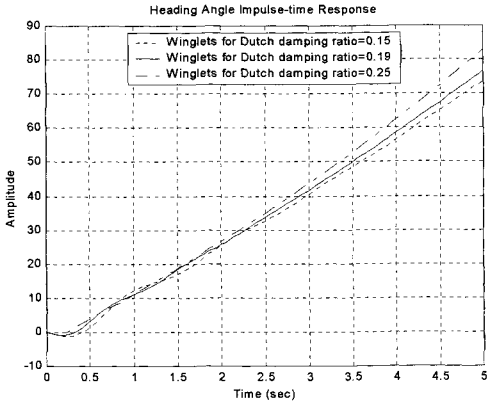

Fig. 41 Heading Angle Response After an Impulse Perturbation

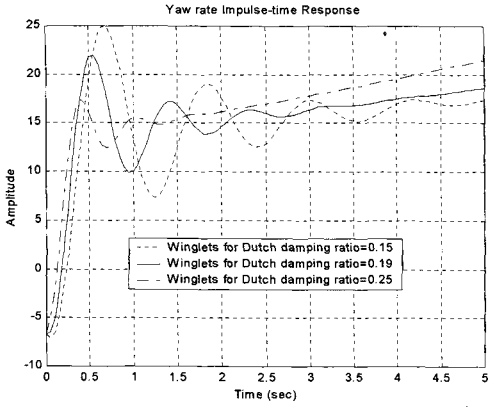

Fig. 39 Yaw Rate Response After an Impulse Perturbation

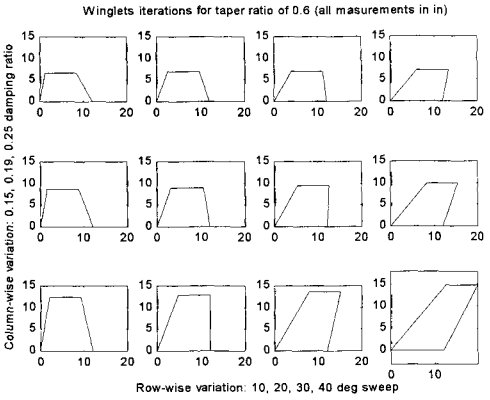

Fig. 42 Winglets iterations for Dutch damping ratios of 0.15, 0.19 and 0.25 (column-wise) and sweep leading edge of 10°, 20°, 3 and 40° respectively (row-wise)